J Fluoresc (2009) 19:191–201
DOI 10.1007/s10895-008-0402-6

ORIGINAL PAPER

Photophysical Properties of Lanthanide Hybrids Covalently Bonded To Functionalized MCM-41 by Modified Aromatic Carboxylic Acids

Ying Li · Bing Yan

Received: 27 May 2008 / Accepted: 14 July 2008 / Published online: 23 July 2008

Abstract MCM-41 mesoporous silica has been functionalized with aromatic carboxylic acids salicylic acid (Sal) and 2-hydroxyl-3-methylbenzoic acid (HMBA) through co-condensation approach of tetraethoxysilane (TEOS) in the presence of the cetyltrimethylammonium bromide (CTAB) surfactant as a template. Organic ligands salicylic acid or 2-hydroxyl-3-methylbenzoic acid grafted to the coupling agent 3-(triethoxysilyl)-propyl isocyanate (TEPIC) was used as the precursor for the preparation of an organic–inorganic hybrid materials. Novel organic–inorganic mesoporous luminescent hybrid containing Ln^{3+} (Tb^{3+}, Eu^{3+}) complexes covalently attached to the functionalized ordered mesoporous MCM-41, which were designated as Ln-Sal-MCM-41 and Ln-HMBA-MCM-41, respectively, were obtained by sol–gel process. The luminescence properties of these resulting materials were characterized in detail, and the results reveal that luminescent mesoporous materials have high surface area, uniformity in the mesopore structure and good crystallinity. Moreover, the mesoporous material covalently bonded Tb^{3+} complex (Tb-Sal-MCM-41 and Tb-HMBA-MCM-41) exhibit the stronger characteristic emission of Tb^{3+} and longer lifetime than the corresponding Eu-containg materials Eu-Sal-MCM-41 and Eu-HMBA-MCM-41 due to the triplet state energy of modified organic ligands Sal-TEPIC and HMBA-TEPIC match with the emissive energy level of Tb^{3+} very well. In addition, the luminescence lifetime and emission quantum efficiency of $^5D_0$ Eu^{3+} excited state also indicates the efficient intramolecular energy transfer process in Tb-SAL-MCM-41 and Tb-HMBA-MCM-41.

Y. Li · B. Yan (✉)
Department of Chemistry, Tongji University,
Shanghai 200092, People's Republic of China
e-mail: byan@tongji.edu.cn

Keywords Luminescent mesoporous material · Covalently bonded · Lanthanide · Photophysical property

Introduction

Luminescent materials, especially lanthanide (Tb^{3+}, Eu^{3+}) complexes have characteristic luminescence properties and give sharp, intense emission lines upon ultraviolet light irradiation, because of the effective intramolecular energy transfer from the coordinated ligands to the luminescent central lanthanide ion [1–3]. The interest in the photophysical properties of lanthanide complexes which act as optical centers in luminescent hybrid materials has grown considerably since Lehn asserted that such complexes could be seen as light harvest supramolecular devices [4]. Therefore, they are expected to be promising luminescent dopants for the preparation of hybrid phosphors and other optical sources. In recent years, lanthanide organic–inorganic hybrid materials, incorporation of rare earth complexes in the inorganic matrices have attracted considerable interest, and the luminescence properties of lanthanide complexes supported on a solid matrix have been studied extensively because their photophysical properties could be modified by interaction with the host structure [5]. According to the chemical nature or different synergy between components, hybrids can be categorized into two main classes. The first class concerns all systems where no covalent bond is present between organic and inorganic parts but only weak interactions (such as hydrogen bonding, van der Waals force or electrostatic forces) [6, 7], the corresponding conventional doping methods seems hard to prohibit the problem of quenching effect on luminescent centers due to the high vibration energy of the surrounding hydroxyl groups. Our research group is concentrated on covalently grafting the

ligands to the inorganic networks in which lanthanide complexes luminescent centers are bonded with a siloxane matrix through Si–O linkage using different modified routes, including the modification of active amino group, hydroxyl groups and carboxyl groups with coupling agent, etc. [8–14]. These studies indicate that the thermal stabilities and photophysical properties of the lanthanide complexes were improved by the matrixes. So far, the incorporation of luminescent lanthanide complexes in solid matrices is of wide spread interest in material science as it allows construction of functional materials with various optical properties [15].

Due to its peculiar characteristics, large internal surface area and favorable uniformity and easily controlled size of the pore, the ordered mesoporous molecular sieve MCM-41 has attracted considerable interest in physics, chemistry, materials science and other relevant areas. These properties together with the thermal and mechanical stabilities make it as an ideal host for incorporation of active molecules and some work has already been devoted on this field [16–19]. For example, Zink et al. took advantage of the different chemical and physical properties of the regions in the sol–gel films and developed new strategies to place the active molecules, e.g. lanthanide complex luminescent molecules, in desired inorganic silicate framework [20]. Mitchell-Koch et al. [21]. immobilized europium complexes within porous organic polymer hosts, and obtained luminescent materials potentially suitable for chemical sensing. As a good host material, studies of the encapsulation and assembly of guest molecules in the mesoporous channels have been very extensive [22–24]. Recently, Carlos et al. [25]. have reported the syntheses of MCM-41 mesoporous materials covalently bonded with ternary europium complexes. It is shown that the promising visible-luminescent properties can be obtained by linking the ternary europium complexes to the mesoporous materials. However, the synthesis and luminescence properties of MCM-41 mesoporous materials covalently bonded with lanthanide complexes by the modified aromatic carboxylic acids have not been explored to date.

In this work, we report a direct synthesis of two kinds of aromatic carboxylic acids functionalized MCM-41 mesoporous hybrid materials (Sal-MCM-41 and HMBA-MCM-41), in which salicylic acid (Sal) and 2-hydroxyl-3-methylbenzoic acid (HMBA) were covalently bonded to the framework of MCM-41 by co-condensation of the modified organic groups (denoted as Sal-TEPIC and HMBA-TEPIC) and the tetraethoxysilane (TEOS) by using the cetyltrimethylammonium bromide(CTAB) surfactant as template. The luminescent lanthanide (Tb^{3+}, Eu^{3+}) complexes on functionalized MCM-41 with modified aromatic carboxylic acid ligands (denoted as Ln-Sal-MCM-41 and Ln-HMBA-MCM-41, Ln=Tb, Eu) were obtained by introducing Ln^{3+} into the Sal-MCM-41 and HMBA-MCM-41 hybrid materials through covalent bond assembling method. Full characterization and detail studies of luminescence properties of all these synthesized materials were investigated in relation to guest–host interactions between the organic complex and the silica matrix.

Experimental

Materials

Cetyltrimethylammonium bromide (CTAB, Aldrich), tetraethoxysilane (TEOS, Aldrich), 3-(triethoxysilyl)-propyl isocyanate (TEPIC, Lancaster), salicylic acid (Sal), 2-hydroxyl-3-methylbenzoic acid (HMBA) and ethanol were used as received. The solvent tetrahydrofuran (THF) was used after desiccation with anhydrous calcium chloride.

$LnCl_3$ (Ln=Tb, Eu) ethanol solution (EtOH) was prepared as follows: the rare earth oxide (Tb_4O_7, Eu_2O_3) was dissolved in concentrated hydrochloric acid (HCl),and the surplus HCl was removed by evaporation. The residue was dissolved with anhydrous ethanol. The concentration of the rare earth ion was measured by titration with a standard ethylenediamine tetraacetic acid (EDTA) aqueous solution.

Synthetic procedures

Preparation of Sal-functionalized MCM-41 mesoporous material (Sal-MCM-41)

The modified salicylic acid (Sal-TEPIC) was prepared as follows: salicylic acid (Sal; 1 mmol, 0.138 g) was first dissolved in 20 ml of dehydrate tetrahydrofuran (THF). 3-(triethoxysilyl)-propyl-isocyanate (TEPIC; 1.1 mmol, 0.26 g) was dropwise added into the refluxing solution with stirring. The mixture was heated at 65 °C in a covered flask for approximately 20 h at the nitrogen atmosphere. After isolation and purification, a yellow oil sample Sal-TEPIC was obtained. Anal: calcd. for Sal-TEPIC ($C_{17}H_{27}O_7NSi$): C, 52.90; H, 7.01; N, 3.64%. Found: C, 52.61; H, 7.21; N, 3.68%. ^1H NMR ($CDCl_3$): δ 14.35(1H,s), 8.40(1H,d), 7.87 (1H,t), 6.79(1H,d), 6.26(1H, t), 4.16(1H,t), 3.65(2H,m), 3.45 (1H,d), 3.28(2H,s), 1.77(8H,m), 1.15(4H,d), 1.05(4H,s)

The mesoporous hybrid material Sal-MCM-41 was synthesized as follows: CTAB (1.1 g) was dissolved in concentrated $NH_3{\cdot}H_2O$ (12 ml), to which demonized water (26 ml), TEOS (5.5 ml), and Sal-TEPIC were added with the following molar composition: 0.12 CTAB:0.5 $NH_3{\cdot}H_2O$:0.96 TEOS:0.04 Sal-TEPIC:58.24 H_2O.The mixture was stirred at room temperature for 24 h and transferred into a Teflon bottle sealed in an autoclave, which was then heated at 100 °C for 48 h. Then the solid product was filtrated, washed thoroughly with deionized water, and air-dried for 12 h at

room temperature. Removal of the surfactant CTAB was conducted by Soxhlet extraction with ethanol for 2 days to give the sample denoted as Sal-MCM-41.

Preparation of HMBA-functionalized MCM-41 Mesoporous material (HMBA-MCM-41)

A typical procedure for the modification of 2-hydroxyl-3-methylbenzoic acid (HMBA) to HMBA-TEPIC: HMBA (1 mmol, 0.153 g) was dissolved in 15 ml of acetone at argon atmosphere. 3-(triethoxysilyl)-propyl isocyanate (1.1 mmol, 0.26 g) was added dropwise into the solution with stirring. The mixture was heated at 60 °C in a covered flask for approximately 16 h. The coating liquid was concentrated to remove the solvent acetone using a rotary vacuum evaporator and the yellow slimy liquid sample was obtained. And then the yellow liquid sample was dissolved in absolute ethanol, and 20 ml of hexane was added into the solution to precipitate. Moreover, the solution was filtrated and white powder was obtained. The above procedures of dissolution and filtration were repeated three times. At last the pure white powder was obtained and dried in a vacuum. HMBA-TEPIC ($C_{18}H_{29}NO_7Si$): Element analysis data: *Anal.* Calcd.: C, 54.17; H, 7.31; N, 3.50. Found: C, 54.40; H, 7.09; N, 3.31. ^{1}HNMR($CDCl_3$): δ0.64(2H, m), 1.25(9H, t), 1.68(2H, m), 2.30(3H, s), 3.18(2H, m), 3.84 (6H, m), 4.81(1H, t), 6.83(1H, d), 7.38(1H, d), 7.79(1H, d), 10.80(1H, s).

Preparation of MCM-41 mesoporous material covalently bonded with the lanthanide (Ln^{3+}) complexes (denoted as Ln-Sal-MCM-41 and Ln-HMBA-MCM-41, respectively. Ln=Tb, Eu)

The sol–gel-derived hybrid mesoporous material Ln-Sal-MCM-41 was prepared as follows: While being stirred, Sal-MCM-41 was soaked in an appropriate amount of $LnCl_3$ ethanol solution with the molar ratio of Ln^{3+}: Sal-TEPIC being 1:3. The mixture was heated under reflux for 12 h, followed by filtration and extensive washing with EtOH. The resulting Ln-Sal-MCM-41 was dried at 60 °C under vacuum overnight.

The synthesis procedure for Ln-HMBA-MCM-41was similar to that of Ln-Sal-MCM-41 except that Sal-TEPIC was replaced by HMBA-TEPIC. And the two hybrid mesoporous products were obtained as outlined in Fig. 1.

Characterization

FI-IR spectra were recorded within the 4000–400 cm^{-1} region on an infrared spectrophotometer with the KBr pellet technique. ^{1}H NMR spectra were recorded in $CDCl_3$ on a Bruker AVANCE-500 spectrometer with tetramethylsilane

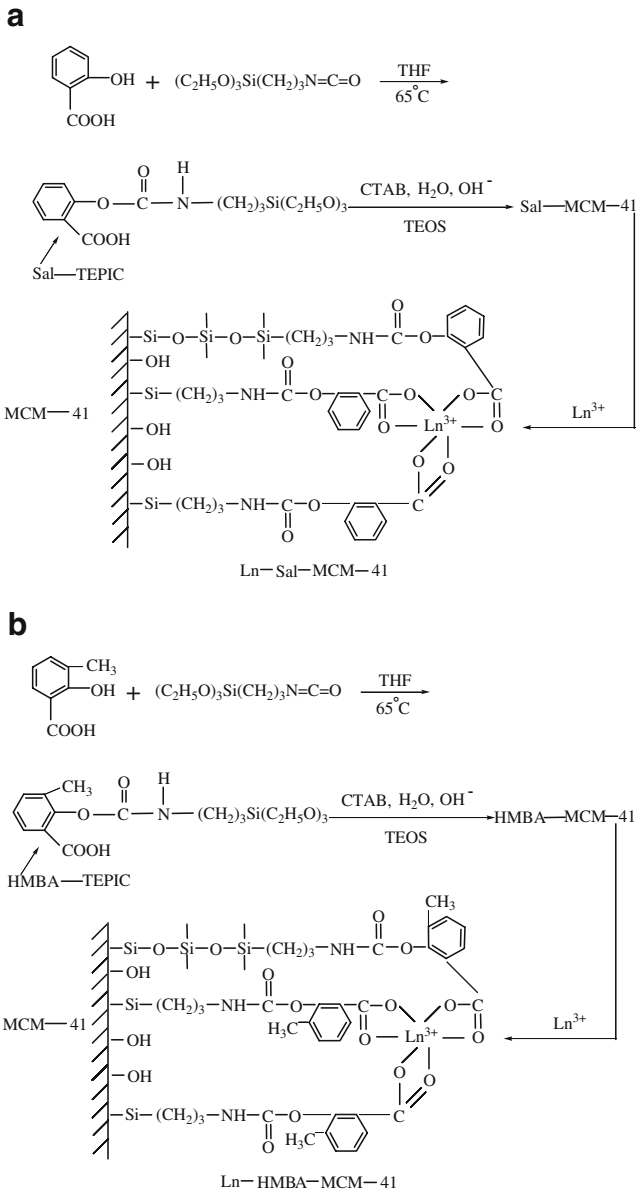

Fig. 1 Synthesis procedure and predicted structure of Ln-Sal-MCM-41 (**a**) and Ln-HMBA-MCM-41 (**b**) (Ln=Tb, Eu)

(TMS) as internal reference. Elemental analyses (C, H, N) were determined with an Elementar Cario EL elemental analyzer. The Ultraviolet absorption spectra were taken with an Agilent 8453 spectrophotometer. X-ray powder diffraction patterns were recorder on a Rigaku D/max-rB diffractometer equipped with a Cu anode in a 2θ range from 0.6° to 6°. Nitrogen adsorption/desorption isotherms were measured at the liquid nitrogen temperature, using a Nova 1000 analyzer. Surface areas were calculated by the Brunauer–Emmett–Teller (BET) method and pore size distributions were evaluated from the desorption branches of the nitrogen isotherms using the Barrett–Joyner–Halenda (BJH) model. The fluorescence excitation and emission

Table 1 The main bands and their assignments of IR spectra for hydroxyl compounds, TESPIC and modified bridge ligands

Compounds	ν(OH)	ν(CH_2)	ν(C=O)	ν(N=C=O)	ν(N–H)	δ(N–H)	ν(C–N)	ν(TEPIC-C)
TESPIC		2,902–2,979	1,637	2,269–2,365			1,266	1,169
Sal	3,240							
Sal-TEPIC		2,921–2,979	1,652		3,056	1,491	1,251	1,200
HMBA	3,252							
HMBA-TEPIC		2,895–2,979	1,665		3,065	1,547	1,252	1,155

spectra were obtained on a RF-5301 spectrophotometer (wavelength resolution was 0.5 nm). Luminescence lifetime measurements were carried out on an Edinburgh FLS920 phosphorimeter using a 450 W xenon lamp as excitation source. Scanning electronic microscope (SEM) was measured on Philip XL30.

Results and discussion

The IR spectra for the modified bridge ligands (Sal-TEPIC, HMBA-TEPIC) were compared to hydroxyl compounds Sal, HMBA and cross linking TESPIC molecule. The main data were given in Table 1. There are apparent characteristic absorption peaks (3,240, 3,452 cm^{-1}) of hydroxyl groups in the IR spectra of Sal and HMBA, respectively. Nevertheless, these bands can not be observed in the modified ligands (Sal-TEPIC, HMBA-TEPIC). Besides, the occurrence of the grafting reaction was also evidenced by the bands about 1,652 cm^{-1} (Sal-TEPIC) and 1,665 cm^{-1} (HMBA-TEPIC) due to the absorption of amide groups (–CONH–). All of above data suggest that 3-(triethoxysilyl)-propyl isocyanate has been successfully grafted on to hydroxyl group of Sal and HMBA, respectively. Compared the IR spectra, the absorption peaks at 2,250, 2,275 cm^{-1} for N=C=O of TESPIC disappeared in the IR spectra of Sal-TEPIC and HMBA-TEPIC. Figure 2 shows the FTIR spectra of Sal-MCM-41 and HMBA-MCM-41. It can be clearly seen that the formation of the Si–O–Si framework is evidenced by the bands located at around 1,081 cm^{-1} (ν_{as}, Si–O), 800 cm^{-1} (ν_s, Si–O), and 460 cm^{-1}(δ, Si–O–Si; ν represents stretching, δ in plane bending, s symmetric, and as asymmetric vibrations), indicate the absorption of siloxane bonds. Furthermore, the peaks at around 1,626 and 1,388 cm^{-1} originating from –CONH– group of the modified organic ligands, can also be observed in hybrid mesoporous materials Sal-MCM-41 and HMBA-MCM-41, which is consistent with the fact that the organic group in the framework remains intact after both hydrolysis-condensation reaction and the surfactant extraction procedure [26].

The power XRD, especially small-angle X-ray diffraction (SAXRD) patterns and nitrogen adsorption/desorption isotherms are popular and efficient methods to characterize highly ordered mesoporous material with hexagonal symmetry of the space group *p6mm*. The SAXRD patterns of a pure MCM-41mesporous silicon(a) (which prepared according to reference [27, 28]), Eu-Sal-MCM-41 (b), Tb-Sal-MCM-41(c), Eu-HMBA-MCM-41(d) and Tb-HMBA-MCM-41(e) are presented in Fig. 3. For all materials, the patterns clearly show the order of the hexagonal array of the MCM-41 structure and exhibit distinct Bragg peaks in the 2θ range of 0.6–6°, which can be indexed as (100), (110), and (200) reflections. Compared with the SAXRD pattern of MCM-41, the d_{100} spacing values of Ln-Sal-MCM-41 and Ln-HMBA-MCM-41(Ln=Tb, Eu) are nearly unchanged (see Table 2), indicating that the framework hexagonal ordering has been retained very well upon the introduction of Ln^{3+} [29, 30]. In addition, it is worth noting that lanthanide-complex functionalized materials appear decreasing in diffraction intensity as compared with the pure MCM-41, which is probably due to the presence of guest moieties inside the pore channels of host MCM-41 material, resulting in the decrease of the mesoporous order, but not the collapse in the pore structure of mesoporous materials [31].

N_2 adsorption-desorption isotherms are used as a macroscopic average measurement for exploring surface area, pore diameter, and pore volume of the material. The N_2 adsorption-desorption isotherm and pore size distribution for pure MCM-41(a), Eu-Sal-MCM-41(b), Tb-Sal-

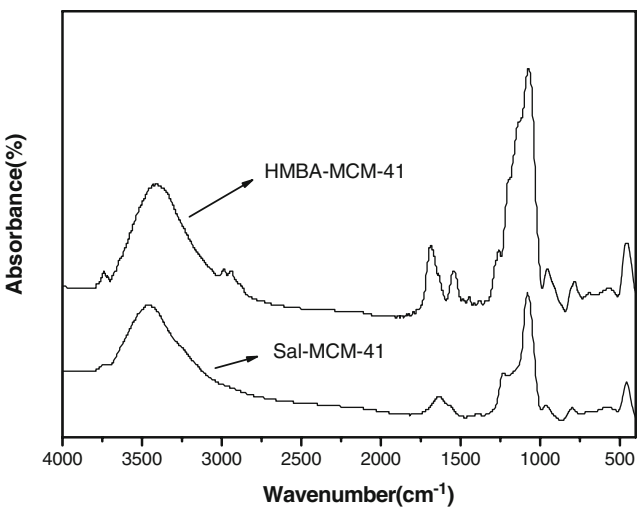

Fig. 2 IR spectra for Sal-MCM-41 and HMBA-MCM-41

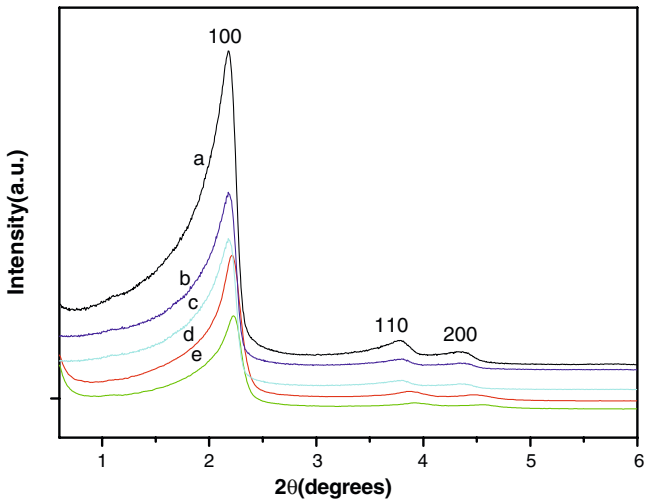

Fig. 3 SAXRD patterns of a pure MCM-41mesporous silicon (*a*), Eu-Sal-MCM-41 (*b*), Tb-Sal-MCM-41 (*c*), Eu-HMBA-MCM-41 (*d*) and Tb-HMBA-MCM-41 (*e*)

MCM-41 (c), Eu-HMBA-MCM-41(d) and Tb-HMBA-MCM-41(e) are shown in Fig. 4. They all display type IV isotherms with H1-type hysteresis loops at low relative pressure according to the IUPAC classification, [32–35] characteristic of mesoporous materials with highly uniform size distributions. From the two branches of adsorption-desorption isotherms, the presence of a sharp adsorption step in the P/P_0 region from 0.3–0.5 and a hysteresis loop at the relative pressure $P/P_0>0.35$ shows that all materials process a well defined array of regular mesopores. The specific area and the pore size have been calculated by using Brunauer–Emmett–Teller (BET) and Barrett–Joyner–Halenda (BJH) methods, respectively. And the structure data of all these mesoporous materials (BET surface area, total pore volume, and pore size, etc.) were summarized in Table 2. It can be clearly seen that all the mesoporous hybrid materials exhibit a smaller specific area and a slightly smaller pore size and pore volume in comparison with those of pure MCM-41, which might be due to the presence of organic ligand on the pore surface and the co-surfactant effect of Sal-TEPIC (or HMBA-TEPIC), which interacts with surfactant and reduces the diameter of the micelles [36, 37].

Figure 5 gives the scanning electron micrograph (SEM) of the mesoporous material Tb-Sal-MCM-41(A) and Tb-HMBA-MCM-41(B). It demonstrates that homogeneous, molecular-based materials were obtained because of strong covalent bonds bridging between the inorganic and organic phase, and that they composed quite uniformly so that the two phases can exhibit their distinct properties together. The hybrid material with doped lanthanide complexes generally experiences phase separation phenomena [38]. Furthermore, comparing the two SEM pictures, there exist distinctions for the two kinds of terbium mesoporous hybrid material from each other, which may be due to the difference of the precursor molecules.

Luminescence measurements have been carried on these lanthanide-complexes functionalized hybrid mesoporous materials at room temperature. The efficient ligands to the central ion energy transfer in the two kinds of mesoporous hybrids are investigated by energy difference between the triplet states of organic ligands and the resonance energy level of the central Ln^{3+}(Tb^{3+}, Eu^{3+}) ion. According to the energy transfer and intramolecular energy mechanism, [39, 40] the most important factor influencing the luminescence properties of rare earth complexes is the intramolecular energy transfer efficiency, which mainly depends on the two energy transfer processes. [41] One is from lowest triplet level of ligands to the emissive energy level of Ln^{3+} ion by the Dexter's resonant exchange interaction theory; [42, 43] the other is the reverse energy transition by the thermal deactivation mechanism. And the energy transfer rate constants (k_T) are dependent on the energy difference (ΔE (T_r–Ln^{3+})) between the lowest triplet level energy of ligands and the resonant emissive energy of Ln^{3+}. Based on the above two facets, the conclusion can be drawn that ΔE (T_r–Ln^{3+}) can have contrast influence on the two energy transfer process mentioned, and there should exist an optimal energy difference between the triplet position of Sal-TEPIC (or HMBA-TEPIC) and the emissive energy level Ln^{3+} (Tb, Eu), the larger or the smaller ΔE (T_r–Ln^{3+}) value will decrease the luminescence properties of rare earth. Thus, the energy difference between the lowest triple state energy of the modified ligand Sal-TEPIC (24,038 cm^{-1}),

Table 2 Textural data of MCM-41, Ln-Sal-MCM-41 and Ln-HMBA-MCM-41 (Ln=Tb, Eu)

Sample	d_{100} (nm)	S_{BET} (m^2/g)	V (cm^3/g)	D_{BJH} (nm)	A_0	t
MCM-41	4.15	1028	0.81	3.13	4.79	1.66
Eu-HMBA-MCM-41	4.10	950	0.63	2.65	4.73	2.08
Tb-HMBA-MCM-41	3.92	966	0.65	2.70	4.53	1.83
Eu-Sal-MCM-41	4.08	872	0.54	2.50	4.71	2.21
Tb-Sal-MCM-41	3.88	941	0.58	2.47	4.48	2.01

d_{100} is the $d(100)$ spacing, a_0 the cell parameter ($a_0=2d_{100}/\sqrt{3}$), S_{BET} the BET surface area, V the pore volume, D the pore diameter, and t the wall thickness, calculated by $a_0 - D$

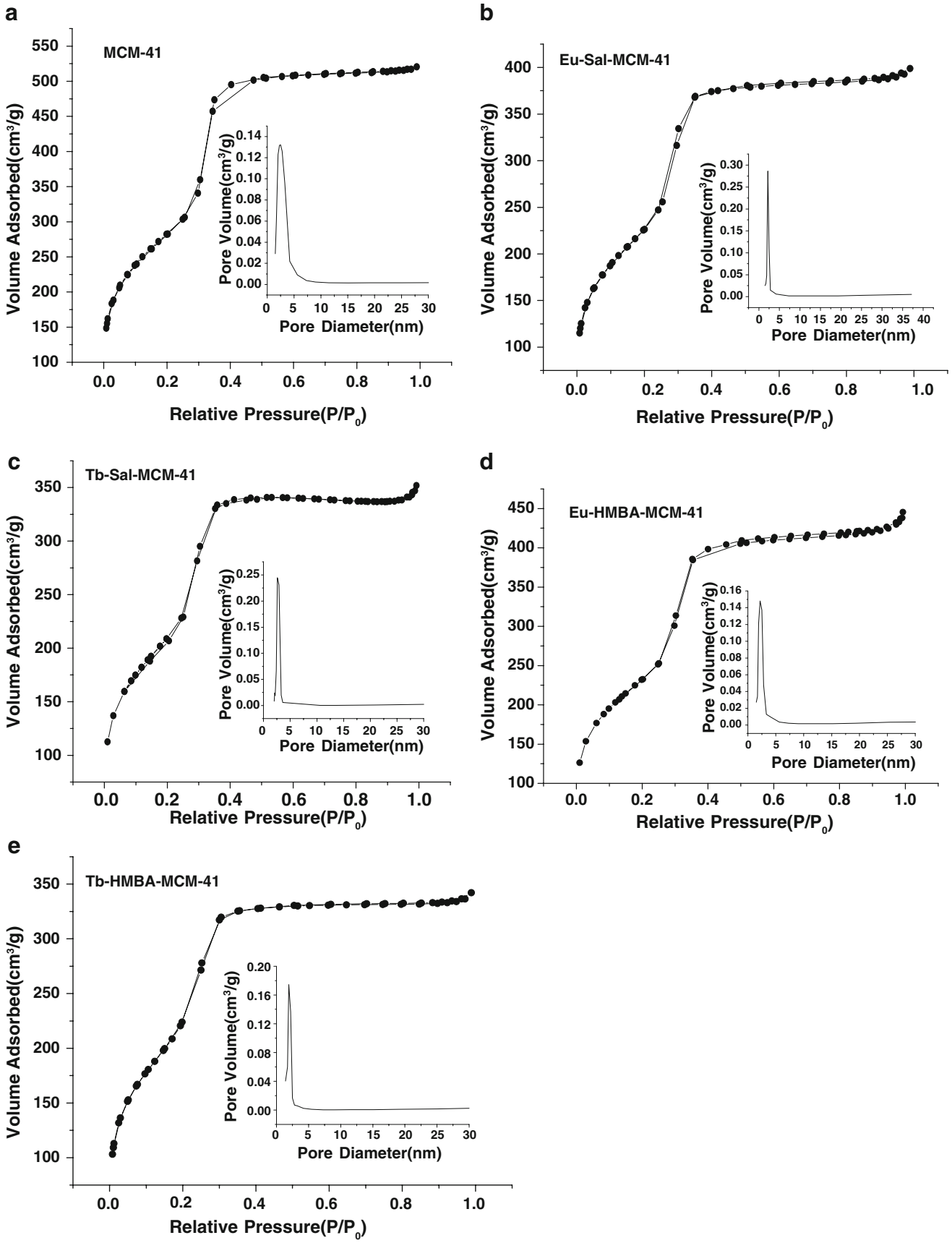
a
MCM-41
Volume Adsorbed(cm³/g)
Relative Pressure(P/P0)
Pore Volume(cm³/g)
Pore Diameter(nm)
b
Eu-Sal-MCM-41
Volume Adsorbed(cm³/g)
Relative Pressure(P/P0)
Pore Volume(cm³/g)
Pore Diameter(nm)
c
Tb-Sal-MCM-41
Volume Adsorbed(cm³/g)
Relative Pressure(P/P0)
Pore Volume(cm³/g)
Pore Diameter(nm)
d
Eu-HMBA-MCM-41
Volume Adsorbed(cm³/g)
Relative Pressure(P/P0)
Pore Volume(cm³/g)
Pore Diameter(nm)
e
Tb-HMBA-MCM-41
Volume Adsorbed(cm³/g)
Relative Pressure(P/P0)
Pore Volume(cm³/g)
Pore Diameter(nm)

◀ **Fig. 4** N_2 adsorption/desorption isotherms and pore distribution of MCM-41(a), Eu-Sal-MCM-41(b), Tb-Sal-MCM-41 (c), Eu-HMBA-MCM-41(d) and Tb-HMBA-MCM-41(e)

HMBA-TEPIC (23,530 cm^{-1}) and the resonance energy levels of Tb^{3+} ($^5D_4$, 20,430 cm^{-1}), Eu^{3+} ($^5D_0$, 17,250 cm^{-1}) were calculated, and it can be predicted that the triplet state energy of the modified ligands is more suitable for the luminescence of Tb^{3+} ion than Eu^{3+} in the resulting materials. So, the hybrid mesoporous materials containing Tb^{3+} exhibit the better luminescence properties.

Figure 6 shows the excitation and emission spectra of Tb-Sal-MCM-41(A) and Tb-HMBA-MCM-41(B) mesoporous material. The excitation spectrum, monitoring the strongest emission band of the Tb^{3+} ion at 545 nm, presents a large broad band between 250 and 450 nm in the two materials. The broad band is attributed to the light absorption by the modified organic ligand. From the emission spectra, characteristic Tb^{3+} ion emissions are observed. It can be clearly seen that main bands in the 450–650 nm range,

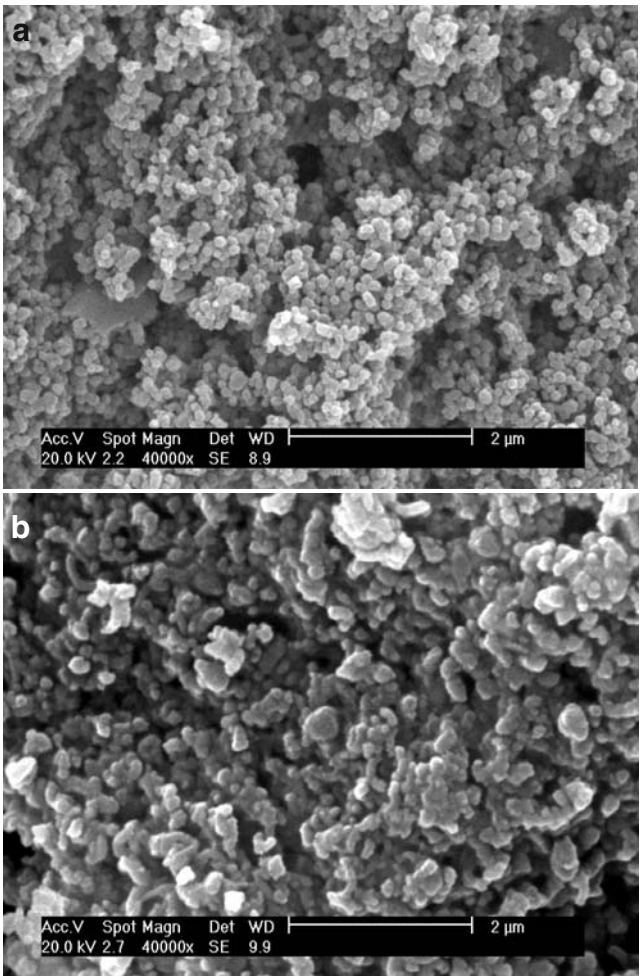

Fig. 5 Scanning electron micrograph (*SEM*) of Tb-Sal-MCM-41 (**a**) and Tb-HMBA-MCM-41 (**b**)

which are assigned to the $^5D_4 \rightarrow {}^7F_j$ (j=6–3) transitions at around 487, 544, 582, 620 nm, respectively. As a result, the strong green luminescence was observed in the emission spectra which indicated that the effective energy transfer took place between the modified organic ligands (Sal and HMBA) and the chelated Tb^{3+} ions. The hybrid mesoporous materials show relatively strong emission due to the chemically covalently bonded molecular Si–O network structure between the complex and the mesoporous silica. Furthermore, the luminescence intensities of the $^5D_4 \rightarrow {}^7F_5$ transition for Tb-Sal-MCM-41(A) and Tb-HMBA-MCM-41(B) were compared. The relative intensity of Tb-HMBA-MCM-41 mesoporous material is stronger than that of Tb-Sal-MCM-41, indicates that the modified ligand HMBA-TEPIC is the most efficient for Tb^{3+} ion and could sensitize its corresponding green emission due to the proper energy level match.

The fluorescent excitation and emission spectra of mesoporous materials containing Eu^{3+} ion are given in Fig. 7. The excitation spectrum was obtained by monitoring the emission of Eu^{3+} at 613 nm and dominated by a distinguished band centered at 324 nm. In addition, the excitation spectrum of the two mesoporous materials exhibit $\pi \rightarrow \pi^*$ electron transition of organic ligand from 220 nm to 450 nm, and a peak at around 400 nm can be observed due to the $f \rightarrow f$ absorption transition ($^7F_0 \rightarrow {}^5D_2$) of Eu^{3+} ion. The emission lines of Eu-Sal-MCM-41(A) and Eu-HMBA-MCM-41(B) were mainly originated from $^5D_0 \rightarrow {}^7F_2$, $^5D_0 \rightarrow {}^7F_4$ transitions at 613, and 703 nm of Eu^{3+}. The $^5D_0 \rightarrow {}^7F_2$ transition is a typical electric dipole transition and strongly varies with the local symmetry of Eu^{3+} ions, while the $^5D_0 \rightarrow {}^7F_1$ transition corresponds to a parity-allowed magnetic dipole transition, which is so weak that can not be seen clearly from the emission spectra of the samples. In addition, among these transitions, $^5D_0 \rightarrow {}^7F_2$ transition shows strong emission, suggesting the chemical environment around Eu^{3+} ions is in low symmetry. [44, 45] As a consequence, both Eu-containing hybrid mesoporous materials can not give the same high emission intensities as the materials containing Tb^{3+}, indicting that the triplet state energy of the modified ligand Sal-TEPIC and HMBA-TEPIC matches with the emissive energy level of Tb^{3+} better than that of Eu^{3+}. The luminescence decay profiles relative to Ln-Sal-MCM-41 and Ln-HMBA-MCM-41 (Ln=Tb, Eu) could be fitted with single exponentials, from which the luminescence lifetimes were calculated to confirm that all the Ln^{3+} ions occupy the same average coordination environment. The luminescent lifetime data of all the Tb^{3+} mesoporous materials present the longer lifetime than Eu^{3+} ion mesoporous materials (see Table 3).

Furthermore, we selectively determined the emission quantum efficiencies (η) of the $^5D_0$ europium ion excited state for Eu^{3+} hybrids on the basis of the emission spectra

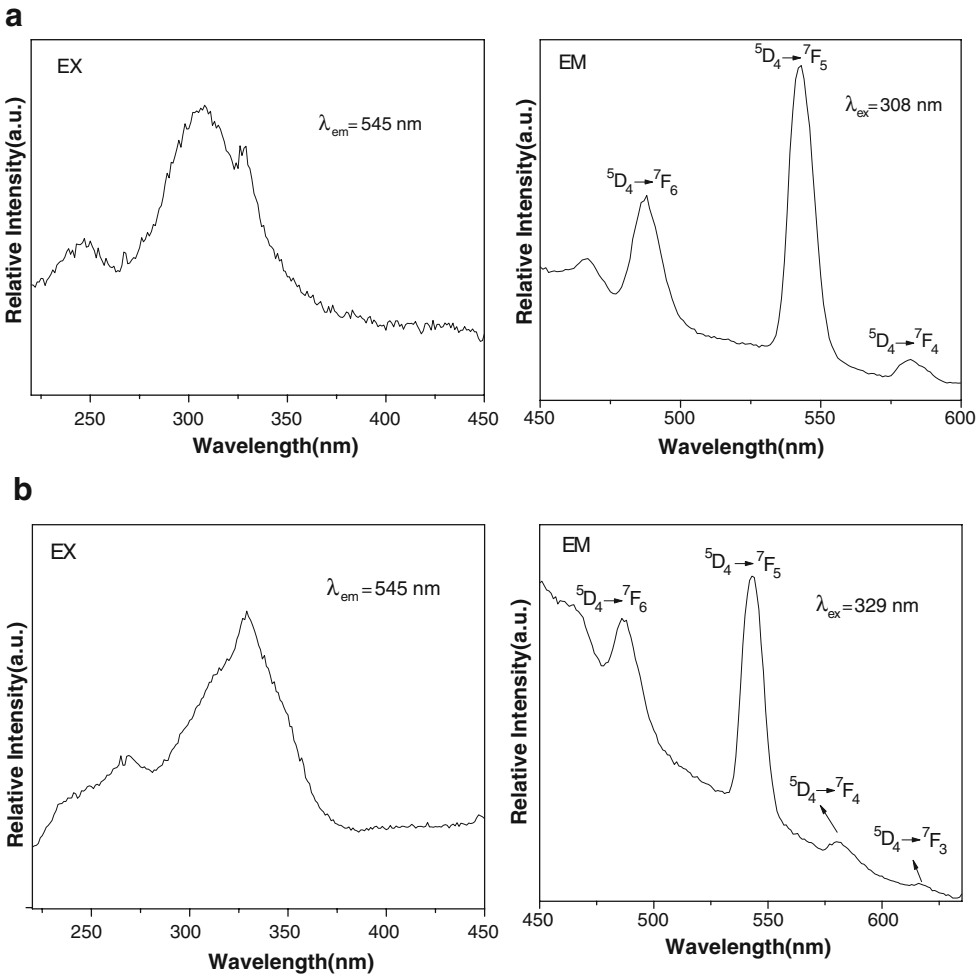

Fig. 6 The excitation and emission spectra of Tb-Sal-MCM-41 (**a**) and Tb-HMBA-MCM-41 (**b**)

and lifetimes of the $^5D_0$ emitting level. Assuming that only nonradiative and radiative processes are essentially involved in the depopulation of the $^5D_0$ states, η can be defined as follows [46]:

$$\eta = \frac{A_r}{A_r + A_{nr}} \tag{1}$$

Where A_r and A_{nr} are radiative and nonradiative transition rates, respectively. Since the magnetic dipole transition $^5D_0 \rightarrow {}^7F_1$ is relatively insensitive to the chemical environments around the Eu^{3+} ion, and thus can be considered as a reference for the whole spectrum. The Einstein's coefficient of spontaneous emission (A_{0J}) can be calculated according to the relation [47].

$$A_{0J} = A_{01}(I_{0J}/I_{01})(\nu_{01}/\nu_{0J}) \tag{2}$$

In Eq. 2, I_{01} and I_{0J} are the integrated intensities of the $^5D_0 \rightarrow {}^7F_1$ and $^5D_0 \rightarrow {}^7F_J$ transitions (J=0–4) with ν_{01} and ν_{0J} ($\nu_{0J}=1/\lambda_J$) energy centers respectively. And A_{01} is the Einstein's coefficient of spontaneous emission between the $^5D_0$ and $^7F_1$ levels. On the basis of reference, [48] the value of $A_{01} \approx 50\ s^{-1}$ and the lifetime (τ), radiative (A_r), and nonradiative (A_{nr}) transition rates are related through the following equation:

$$A_{tot} = 1/\tau = A_r + A_{nr} \tag{3}$$

A_r can be obtained by summing over the radiative rates A_{0J} for each $^5D_0 \rightarrow {}^7F_J$ transition

$$A_r = A_{01}\frac{\nu_{01}}{I_{01}}\sum_{J=0}^{4}\frac{I_{0J}}{\nu_{0J}} = \sum_J A_{0J} \tag{4}$$

In addition, the number of coordinated water molecules (n_w) can be estimated from the experimental decay time by the empirical formula [49]:

$$n_w = 1.05(A_{tot} - A_r) \tag{5}$$

According to Eqs 1, 2, 3, 4, 5, the parameters A_r, A_{nr}, n_w and the quantum efficiency values (η), for the $^5D_0$ Eu^{3+} ion excited state in the sample Eu-SAL-MCM-41 can be obtained, as shown in Table 3. The low quantum efficiency of Eu^{3+} in Eu-Sal-MCM-41(η=4.7%) and in Eu-HMBA-MCM-41 (η=10.54%) indicate that the high nonradiative

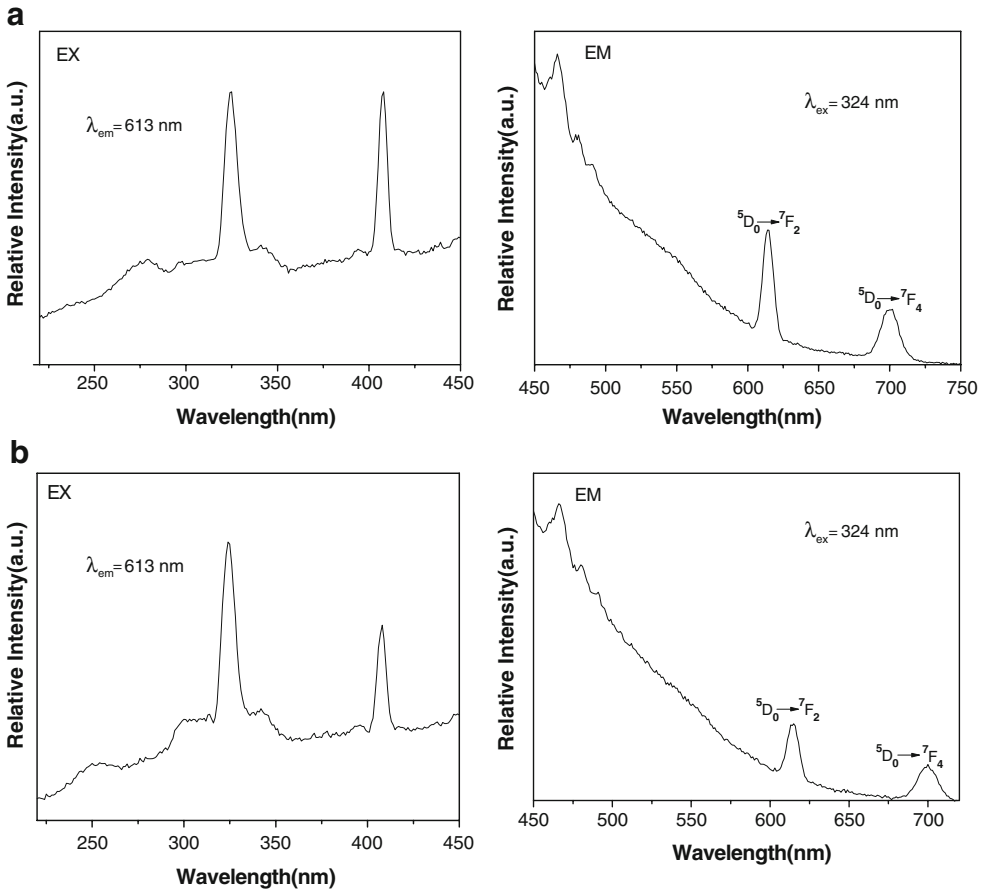

Fig. 7 The excitation and emission spectra of Eu-Sal-MCM-41 (**a**) and Eu-HMBA-MCM-41 (**b**)

transition due to the luminescence quenching of the $^5D_0$ emitting level by the vibration of OH or silanol. Moreover, the triple state energy of the modified ligand Sal-TEPIC and HMBA-TEPIC are not quite suitable for the luminescence of Eu^{3+} ion comparing with Tb^{3+}, suggesting that there is a more efficient intramolecular energy transfer process in Tb-containing materials than in the materials containing Eu^{3+} ion, which resulting in the lower emission quantum efficiency in material Eu-Sal-MCM-41 and Eu-HMBA-MCM-41.

Conclusions

In summary, the lanthanide (Tb^{3+}, Eu^{3+}) complexes have been successfully covalently immobilized in the ordered MCM-41 mesoporous material by the modification of aromatic carboxylic acids salicylic acid (Sal) and 2-hydroxyl-3-methylbenzoic acid (HMBA) with 3-(triethoxysilyl)-propyl isocyanate (TEPIC) using a co-condensation method. The synthesis of Sal-MCM-41(or HMBA-MCM-41) provides a convenient approach of tailoring the surface properties of

Table 3 Photoluminescent data of Ln-Sal-MCM-41 and Ln-HMBA-MCM-41(Ln=Tb, Eu)

	λ_{em} (nm)	λ_{ex} (nm)	I (a.u.)	τ (ms)	$1/\tau$ (s^{-1})	A_r ($ms^{-1}\times10^3$)	A_{nr} ($ms^{-1}\times10^3$)	η (%)	n_w
		486.0	850.920						
Tb-Sal-MCM-41	545	543.0	963.349						
		580.0	258.098	1.24	806	–	–	–	–
		616.0	146.958						
Eu-Sal-MCM-41	613	613.0	144.662	0.31	3226	153.14	307.29	4.7	3
		700.0	95.148						
		488.0	476.081						
Tb-HMBA-MCM-41	545	543.0	746.462	1.08	926	–	–	–	–
		582.0	135.192						
Eu-HMBA-MCM-41	613	614.0	231.776	0.46	2174	229.04	1,944.96	10.54	2
		702.0	124.784						

mesoporous silicates by organic functionalization, and the derivative materials Ln-Sal-MCM-41 and Ln-HMBA-MCM-41 (Ln=Tb, Eu) all retain the mesoporous structures. Further investigation into the luminescence properties of all the resulting mesoporous hybrid materials show that the characteristic luminescence of the corresponding lanthanide ions (Ln^{3+}) through the intramolecular energy transfers from the modified ligand to the lanthanide ions. Meantime, the luminescent lifetime of mesoporous materials indicates the similar feature to the luminescence intensities, elucidating that the triple state energy level of Sal-TEPIC (or HMBA-TEPIC) is more quite suitable for the central Tb^{3+} than Eu^{3+}. Furthermore, it should be emphasized that Ln^{3+} ion are well shielded from its chemical environment and the drawback of limited solubility of the lanthanide complexes could be largely increased during the complexes are covalently linked to the matrices. The method of synthesis can be easily applied to other compounds and different modified organic ligand, the desired properties of mesoporous MCM-41 can be tailored by an appropriate choice of the precursors and the metal ions. In conclusion, the good luminescent properties of these materials, together with the highly ordered hexagonal channel structures and uniform tunable pore sizes of MCM-41 mesoporous materials will expand their applications in optical or electronic areas.

Acknowledgements This work was supported by the National Natural Science Foundation of China (20671072).

References

1. DeSá GF, Malta OL, De Mello Doneg, á C, Simas AM, Longo RL, Santa-Cruz PA, da Silva EF Jr (2000) Spectroscopic properties and design of highly luminescent lanthanide coordination complexes. Coord Chem Rev 196:165
2. Sabbatini N, Guardingli M, Lehn JM (1993) Luminescent lanthanide complexes as photochemical supramolecular devices. Coord Chem Rev 123:201
3. Blasse G (1995) Luminescent materials: is there still news? J Alloy Compd 225:529
4. Lehn JM (1990) Perspectives in supramolecular chemistry—from molecular recognition towards molecular information processing and self-organization. Angew Chem Int Ed Engl 29:1304
5. Serra QA, Rosa ILV, Medeiros CL, Zaniquell MED (1994) Luminescent properties of Eu3+ b-diketonate complexes supported on Langmuir–Blodgett films. J Lumin 60–61:112
6. Tanner PA, Yan B, Zhang HJ (2000) Preparation and luminescence properties of sol–gel hybrid materials incorporated with europium complexes. J Mater Sci 35:4325
7. Koslova NI, Viana B, Sanchez C (1993) Rare-earth-doped hybrid siloxane-oxide coatings with luminescent properties. J Mater Chem 3:111
8. Wang QM, Yan B (2004) From molecules to materials: a new way to construct luminescent chemical bonded hybrid systems based with ternary lanthanide complexes of 1,10-phenanthroline. Inorg Chem Commun 7:1124
9. Zhao LM, Yan B (2005) A novel path to luminescent hybrid molecular materials: modifying the hydroxyl group of 6-hydroxynicotinic acid by grafting to a silica network. Appl Organomet Chem 19:1060
10. Yan B, Zhao LM (2005) Construction of luminescent terbium inorganic/organic molecular-based hybrids from modified functional bridge ligand. Mater Lett 59:795
11. Wang QM, Yan B (2006) Assembly of luminescent hybrids from co-polymers bearing functional 4-vinyl pyridine and europium aromatic carboxylate. J Photochem Photobiol, A: Chem 177:1
12. Wang QM, Yan B (2005) A Novel Way to prepare luminescent terbium molecular-scale hybrid materials: modified heterocyclic ligands covalently bonded with silica.. Cryst Growth Des 5:497
13. Wang QM, Yan B (2005) Construction of lanthanide luminescent molecular-based hybrid material using modified functional bridge chemical bonded with silica. J Photochem Photobiol, A: Chem 175:159
14. Yan B, Wang FF (2007) Molecular design and photo-physics of quaternary hybrid terbium centered systems with novel functional di-urea linkages of strong chemical bonds through hydrogen transfer addition. J Organomet Chem 692:2395
15. Sanchez C, Lebeau B, Chaput F, Boilot JP (2003) Optical properties of functional hybrid organic–inorganic nanocomposites. Adv Mater 15:1969
16. Zhang WH, Shi JL, Wang LZ, Yan DS (2000) Preparation and characterization of ZnO clusters inside mesoporous silica. Chem Mater 12:1408
17. Yu J, Shi JL, Wang LZ, Ruan ML, Yan DS (2001) Preparation of high thermal stability MCM-41 in the low surfactant/silicon molar ratio synthesis systems. Mater Lett 48:112
18. Maschmeyer T, Rey F, Sankar G, Thomas JM (1995) Heterogeneous catalysts obtained by grafting metallocene complexes onto mesoporous silica. Nature 378:159
19. Burch R, Cruise N, Gleeson D, Tsang SC (1996) Surface-grafted manganese-oxo species on the walls of MCM-41 channels—a novel oxidation catalyst. Chem Commun, pp 951–952
20. Minoofar PN, Hernandez R, Chia S, Dunn B, Zink JI, Franville AC (2002) Placement and characterization of pairs of luminescent molecules in spatially separated regions of nanostructured thin films. J Am Chem Soc 124:14388
21. Mitchell-Koch JT, Borovith AS (2003) Immobilization of a Europium Salen complex within porous organic hosts: modulation of luminescence properties in different chemical environments. Chem Mater 15:3490
22. Maria LC, Frances LC, Garcia H, Marti V, Scaiano JC (1996) Intrazeolite photochemistry. 13. Photophysical properties of bulky 2,4,6-triphenylpyrylium and tritylium cations within large- and extra-large-pore zeolites. J Phys Chem 100:18152
23. Xu QH, Li LS, Li B, Yu JH, Xu RR (2000) Encapsulation and luminescent property of tetrakis (1-(2-thenoyl)-3,3,3-trifluoracetate) europium *N*-hexadecyl pyridinium in modified Si-MCM-41. Micropor Mesopor Mater 38:351
24. Gago S, Fernandes JA, Rainho JP, Sá Ferreira RA, Pillinger M, Valente AA, Santos TM, Carlos LD, Ribeiro-Claro PJA, Goncalves IS (2005) Highly luminescent tris(b-diketonate)europium (III) complexes immobilized in a functionalized mesoporous silica. Chem Mater 17:5077
25. Li HR, Lin J, Fu LS, Guo JF, Meng QG, Liu FY, Zhang HJ (2002) Phenanthroline-functionalized MCM-41 doped with europium ions. Micropor Mesopor Mater 55:103
26. Sun LN, Zhang HJ, Peng CY, Yu JB, Meng QG, Fu LS, Liu FY, Guo XM (2006) Covalent linking of near-infrared luminescent ternary lanthanide (Er^{3+}, Nd^{3+}, Yb^{3+}) complexes on functionalized mesoporous MCM-41 and SBA-15. J Phys Chem B 110:7249

27. Zhang JY, Luz Z, Goldfarb D (1997) EPR studies of the formation mechanism of the mesoporous materials MCM-41 and MCM-50. J Phys Chem B 101:7087
28. Hukkamäki J, Suvanto S, Suvanto M, Pakkanen TT (2004) Influence of the pore structure of MCM-41 and SBA-15 silica fibers on atomic layer chemical vapor deposition of cobalt carbonyl. Langmuir 20:10288
29. Bourlinos AB, Karakostas Th, Petridis D (2003) "Side chain" modification of MCM-41 silica through the exchange of the surfactant template with charged functionalized organosiloxanes: an efficient route to valuable reconstructed MCM-41 derivatives. J Phys Chem B 107:920
30. Sun LN, Yu JB, Zhang HJ, Meng QG, Ma E, Peng CY, Yang KY (2007) Near-infrared luminescent mesoporous materials covalently bonded with ternary lanthanide [Er(III), Nd(III), Yb(III), Sm (III), Pr(III)] complexes. Micropor Mesopor Mater 98:156
31. Everett DH (1972) Manual of symbols and terminology for physicochemical quantities and units, appendix ii: definitions, terminology and symbols in colloid and surface chemistry. Pure Appl Chem 31:577
32. Sing KSW, Everett DH, Haul RAW, Moscow L, Pierotti RA, Rouquerol J, Siemieniewska T (1985) Reporting physisorption data for gas/solid systems with special reference to the determination of surface area and porosity. Pure Appl Chem 57:603
33. Lim MH, Stein A (1999) Comparative studies of grafting and direct syntheses of inorganic–organic hybrid mesoporous materials. Chem Mater 11:3285
34. Zhang WH, Lu XB, Xiu JH, Hua ZL, Zhang LX, Robertson M, Shi JL, Yan DS, Holmes JD (2004) Synthesis and characterization of bifunctionalized ordered mesoporous materials. Adv Funct Mater 14:544
35. Peng CY, Zhang HJ, Meng QG, Li HR, Yu JB, Guo JF, Sun LN (2005) Synthesis and luminescence properties of SBA-15 functionalized with covalently bonded ternary europium complex. Inorg Chem Commun 8:440
36. Hu QY, Hampsey JE, Jiang N, Li CJ, Lu YF (2005) Surfactant-templated organic functionalized mesoporous silica with phosphino ligands. Chem Mater 17:1561
37. Ferreira RAS, Carlos LD, Goncalves RR, Ribeiro SJL, Bermudez VD (2001) Energy-transfer mechanisms and emission quantum yields in Eu^{3+}-based siloxane-poly(oxyethylene) nanohybrids. Chem Mater 13:2991
38. Crosby GA, Whan RE, Alire RM (1961) Intramolecular energy transfer in rare earth chelates. Role of the triplet state. J Chem Phys 34:743
39. Yan B, Zhang HJ, Wang SB, Ni JZ (1998) Intramolecular energy transfer mechanism between ligands in ternary rare earth complexes with aromatic carboxylic acids and 1,10-phenanthroline. J Photochem Photobiol, A: Chem 116:209
40. Latva M, Takal H, Mukkala V, Matachescuc C, Rodriguez-Ubisd JC, Kankarea J (1997) Correlation between the lowest triplet state energy level of the ligand and lanthanide (III) luminescence quantum yield. J Lumin 75:149
41. Dexter DL (1953) A Theory of sensitized luminescence in solids. J Chem Phys 21:836
42. Yan B, Zhang HJ, Ni JZ (1998) Photophysical properties of some binary and ternary complexes of rare earth ions with aminobenzoic acids and 1,10-phenanthroline. Monafsh Chem 129:151
43. Miranda Jr P, Zukerman-Schpector J, Isolani PC, Vicentini G, Zinner LB (2002) Synthesis and structure of lanthanide picrates with *trans*-1,3-dithiane-1,3-dioxide. J Alloys Compd 344:141
44. Guo XM, Fu LS, Zhang HJ, Carlos LD, Peng CY, Guo JF, Yu JB, Deng RP, Sun LN (2005) Incorporation of luminescent lanthanide complex inside the channels of organically modified mesoporous silica via template-ion exchange method. New J Chem 29:1351
45. Soares-Santos PCR, Nogueira HIS, Félix V, Drew MGB, Ferreira RAS, Carlos LD, Trindade T (2003) Novel lanthanide luminescent materials based on complexes of 3-hydroxypicolinic acid and silica nanoparticles. Chem Mater 15:100
46. Teotonio ES, Espínola JGP, Brito HF, Malta OL, Oliveria SF, de Foria DLA, Izumi CMS (2002) Influence of the *N*-[methylpyridyl]acetamide ligands on the photoluminescent properties of Eu(III)-perchlorate complexes. Polyhedron 21:1837
47. Carlos LD, Messaddeq Y, Brito HF, Ferreira RAS, Bermudez VD, Ribeiro SJL (2000) Full-color phosphors from europium(III)-based organosilicates. Adv Mater 12:594
48. Hazenkamp MF, Blasse G (1990) Rare-earth ions adsorbed onto porous glass: luminescence as a characterizing tool. Chem Mater 2:105
49. Horrocks W De W, Sudnick DR (1979) Lanthanide ion probes of structure in biology. Laser-induced luminescence decay constants provide a direct measure of the number of metal-coordinated water molecules. J Am Chem Soc 101:334